IEEE Access
Multidisciplinary ⋮ Rapid Review ⋮ Open Access Journal

Received May 7, 2022, accepted May 31, 2022, date of publication June 3, 2022, date of current version June 9, 2022.

Digital Object Identifier 10.1109/ACCESS.2022.3180178

Beamforming Feedback-Based Model-Driven Angle of Departure Estimation Toward Legacy Support in WiFi Sensing: An Experimental Study

SOHEI ITAHARA[1], (Graduate Student Member, IEEE), SOTA KONDO[1], (Graduate Student Member, IEEE), KOTA YAMASHITA[1], (Student Member, IEEE), TAKAYUKI NISHIO[1,2], (Senior Member, IEEE), KOJI YAMAMOTO[1], (Senior Member, IEEE), AND YUSUKE KODA[3], (Member, IEEE)

[1]Graduate School of Informatics, Kyoto University, Kyoto 606-8501, Japan
[2]School of Engineering, Tokyo Institute of Technology, Ookayama, Meguro-ku, Tokyo 152-8550, Japan
[3]Centre of Wireless Communications, University of Oulu, 90014 Oulu, Finland

Corresponding author: Koji Yamamoto (kyamamot@i.kyoto-u.ac.jp)

This work was supported in part by the Research and Development through the Ministry of Internal Affairs and Communications/Strategic Information and Communications R&D Promotion Programme (MIC/SCOPE) under Grant JP196000002, and in part by the Japan Society for the Promotion of Science (JSPS) KAKENHI under Grant JP18H01442.

ABSTRACT In this study, we experimentally validated the possibility of estimating the angle of departure (AoD) using multiple signal classification (MUSIC) with only WiFi control frames for beamforming feedback (BFF), defined in IEEE 802.11ac/ax. The examined BFF-based MUSIC is a model-driven algorithm that does not require a pre-obtained database. This is in contrast with most existing BFF-based sensing techniques, which are data-driven and require a pre-obtained database. Moreover, BFF-based MUSIC affords an alternative AoD estimation method without requiring access to the channel state information (CSI). Extensive experimental and numerical evaluations demonstrate that BFF-based MUSIC can successfully estimate the AoDs for multiple propagation paths. Moreover, the evaluations performed in this study reveal that BFF-based MUSIC, where BFF is a highly compressed version of CSI in IEEE 802.11ac/ax, achieves an error of AoD estimation that is comparable to that of CSI-based MUSIC.

INDEX TERMS Wireless sensing, channel state information, beamforming feedback, MUSIC algorithm.

I. INTRODUCTION

WiFi sensing [1], [2] is envisioned as a technology that adds value to existing wireless local area networks beyond the communication infrastructure. In WiFi sensing, an example of the widely used radio frequency (RF) information is the channel state information (CSI), which is measured in multiple-input multiple-output orthogonal frequency-division multiplexing (MIMO-OFDM) systems [1]. CSI demonstrates a high sensing ability to facilitate CSI-based sensing with a low implementation cost and high sensing accuracy.

Currently, the next-generation WiFi standards task group, IEEE 802.11bf [3], is actively embedding WiFi sensing ability into WiFi standards. In IEEE 802.11bf [3], allowing WiFi sensing with legacy devices (i.e., devices whose physical (PHY) layers are compliant with legacy WiFi standards, such as IEEE 802.11ac/ax [4], [5]) is essential. A challenge in terms of meeting this requirement is that the legacy PHY layer processes and discards CSI, thereby restricting the use of CSI for WiFi sensing.

To address this challenge, beamforming feedback (BFF), which is a compressed version of CSI, has attracted attention as alternative RF information to CSI [6]–[13]. Specifically, BFF includes a highly quantized right singular matrix of the CSI matrix for each subcarrier and subcarrier-averaged stream gain. In IEEE 802.11ac/ax [4], [5], a station (STA) transmits BFFs to an access point (AP) without encryption, which allows an arbitrary WiFi device to obtain the BFFs with medium access control (MAC)-level frame-capturing tools.

The associate editor coordinating the review of this manuscript and approving it for publication was Wei-Wen Hu.

Previous studies [6]–[13] have demonstrated the feasibility of BFF-based sensing in several sensing tasks, such as human localization and respiratory estimation.

However, existing BFF-based sensing literature lacks in the following two aspects: 1) model-driven sensing and 2) comparison of CSI with BFF in terms of the sensing accuracy. For the first aspect, to the best of the authors' knowledge, in the BFF-based sensing literature, no model-driven algorithms exist that geometrically estimate the surrounding environment based on mathematical modeling. Specifically, in existing BFF-based sensing methods [6]–[11], referred to as data-driven methods, sensing tasks are conducted via pattern matching to a pre-obtained training dataset, which comprises the BFF and corresponding actual-measured target labels (e.g., human locations or device locations). Because such generation procedures of training datasets incur tremendous human costs, the cost of data-driven sensing is generally higher than that of model-driven sensing. Therefore, the lack of model-driven methods in BFF-based sensing literature results in significant drawbacks for CSI-based sensing, including model-driven algorithms [14], [15].

This motivated the development of a BFF-based model-driven sensing algorithm that does not require preparation of the dataset. To this end, we revisited model-based sensing in CSI-based sensing literature. A fundamental technique referred to as the multiple signal classification (MUSIC) algorithm [16] was used to estimate the angle of departure (AoD) for each multiple propagation path. AoD is useful for device localization, human detection, human localization, and human tracking [1].

This study demonstrates that an extension of the MUSIC algorithm [16] can be realized using BFF. Specifically, given $\bar{\boldsymbol{\Lambda}}$ and $\boldsymbol{V}_k$ as the subcarrier-averaged stream gain and right singular matrix of the CSI matrix at the kth subcarrier, respectively, noise subspace vectors in the MUSIC algorithm can be estimated as the eigenvectors of a covariance matrix $\sum_k \boldsymbol{V}_k \bar{\boldsymbol{\Lambda}} \boldsymbol{V}_k^{\mathrm{H}}$ with an eigenvalue of zero. In contrast, CSI-based MUSIC generally uses a covariance matrix $\sum_k \boldsymbol{h}_k{}^{\mathrm{H}} \boldsymbol{h}_k$, where $\boldsymbol{h}_k$ represents a row vector of the CSI matrix. Mathematical analyses reveal that the role of the covariance matrix obtained from BFF is the same as that of the covariance matrix obtained from CSI. Our numerical evaluation and extensive experimental evaluations indicate that the BFF-based MUSIC algorithm accurately estimates AoDs and is comparable to the CSI-based MUSIC algorithm.

Regarding the second aspect, to the best of the authors' knowledge, existing BFF-based sensing approaches have not provided sensing-accuracy comparisons between CSI and BFF. Instead of the benefit of the usability of BFF, because BFF is a highly compressed version of CSI, the sensing accuracy of BFF is, in principle, lower than that of CSI. Thus, experimental comparisons of CSI and BFF are essential to assess the feasibility of replacing CSI with BFF. We compared the AoD estimation accuracy of BFF- and CSI-based sensing and revealed that the accuracy of BFF-based sensing is comparable to that of CSI-based sensing. Specifically, in three experimental environments, the median AoD estimation accuracy difference between BFF-based MUSIC and CSI-based MUSIC was found to be smaller than 0.1°.

The contributions of this study are summarized as follows:

- We analytically confirmed that the MUSIC algorithm can be employed using only the BFF frame, specifically $\bar{\boldsymbol{\Lambda}}$ and $\boldsymbol{V}_k$. Noise subspace vectors in the MUSIC algorithm are estimated as eigenvectors of $\sum_k \boldsymbol{V}_k \bar{\boldsymbol{\Lambda}} \boldsymbol{V}_k^{\mathrm{H}}$ with an eigenvalue of zero. This finding indicates that AoD estimation explicitly based on BFF is possible, thereby elucidating the applicability of model-driven BFF-based sensing in various sensing tasks (e.g., human sensing and device localization).
- Through experimental evaluations, we revealed that the AoD estimation accuracy of BFF-based MUSIC is comparable to that of CSI-based MUSIC. This is despite the fact that the BFF procedure defined in IEEE 802.11ac/ax quantizes $\boldsymbol{V}_k$ and $\bar{\boldsymbol{\Lambda}}$ (e.g., 3×2 complex matrix is represented by only 30 bit). That is, we demonstrated the feasibility of model-driven BFF-based sensing as an alternative method without requiring access to CSI. Furthermore, note that this is the first work that compares BFF-based sensing and CSI-based sensing in terms of the sensing accuracy under same experimental environments.

This study focused on the feasibility of the original MUSIC algorithm using BFF and the assessment of the accuracy degradation of BFF with respect to CSI. Thus, a comparison and implementation with more sophisticated CSI-based sensing methods such as [14], data-driven BFF-based sensing methods, and AoD estimation techniques based on observation of the signal itself [17], [18] lie outside the scope of this study.

II. RELATED WORKS

Herein, we present a brief overview of the existing WiFi sensing literature utilizing CSI and BFF, detailing differences between the motivations behind these existing studies and our research. Note that AoD estimation techniques based on an observation of the signal itself [17], [18] are not generally used for WiFi sensing.

A. CSI-BASED SENSING

Owing to the rich sensing capacity of CSI, it has attracted attention in terms of providing RF information for WiFi sensing [1], [2]. Existing CSI-based sensing methods include model-driven methods [1], [2], [14], [15], [19] and data-driven methods [1], [2], [20]. While data-driven methods incur considerable costs for collecting training datasets, model-driven methods are executed without any training dataset, thus resulting in lower implementation costs. A basic approach of model-driven methods is the MUSIC algorithm [14]–[16], which is detailed in Section III-D. Based on the MUSIC algorithm, various extended versions [14], [21], [22] have been proposed.

TABLE 1. Summary of BFF-based WiFi sensing.

	Task	Model/Data driven?	Comparison with CSI-based sensing
[6]–[8], [12], [13]	Human localization	Data-driven	No
[9]	Respiratory rate estimation	Model-driven	No
[10]	Camera image reconstruction	Data-driven	No
[11]	Device localization	Data-driven	No
[13]	AoD estimation	Data-driven	No
This study	AoD estimation	**Model-driven**	**Yes**

However, general WiFi devices discard CSI in the PHY layer, and thus, they cannot conduct CSI-based sensing without remodeling their firmware. Thus, a remodeled firmware (e.g., [23]–[25]) is required to conduct CSI-based sensing. Moreover, few wireless chips permit access to the PHY layer from the remodeled firmware.

B. BFF-BASED SENSING

In contrast to CSI-based sensing, BFF-based sensing, which can be performed using arbitrary devices that are compliant with the IEEE 802.11ac/ax standard, is the focus herein. As mentioned in the previous section, BFFs can be collected via MAC-layer frame capturing without any constraints regarding the firmware. Thus, BFF sensing demonstrates potential as an alternative to CSI in WiFi sensing with legacy devices.

Table 1 summarizes existing BFF-based sensing studies. Most studies [6]–[8], [10]–[13] are categorized as data-driven methods. Only [9] is categorized as a model-driven method. [9] estimated the respiratory rate of a human by focusing on the relationship between the temporal variations of BFF and respiratory rate. However, [9] is a heuristic model and does not provide any propagation model-based analyses. In contrast with these studies, the present study is based on a well-known propagation model [26]. Furthermore, we analytically confirm that the AoD is estimated using BFF via the MUSIC algorithm.

Moreover, this is the first study that presents accuracy comparisons between CSI and BFF. Prior studies [6]–[13] have only provided the accuracy of BFF-based sensing and have not performed comparisons between CSI- and BFF-based sensing. Because BFF includes significant quantization losses, the accuracy of BFF-based sensing is principally inferior to that of CSI-based sensing. Thus, evaluating the degree of accuracy degradation is essential to assess whether BFF serve as an alternative to CSI. Our extensive experimental evaluations revealed that the median of the AoD estimation accuracy of BFF-based MUSIC is comparable to that of CSI-based MUSIC.

III. PRELIMINARIES

A. NOTATIONS

We denote the transpose of a matrix $\boldsymbol{H}$ as $\boldsymbol{H}^{\mathrm{T}}$, its conjugate as $\boldsymbol{H}^{*}$, its Hermitian transpose as $\boldsymbol{H}^{\mathrm{H}}$, and the (i, j) element as $H_{i,j}$. We denote the ith element of a vector $\boldsymbol{a}$ as a_i, and the Euclidean norm as $|\boldsymbol{a}|$. The identity matrix is represented as $\boldsymbol{E}$. The diagonal matrix, whose ith diagonal element is a_i, is represented as $\mathrm{diag}(\boldsymbol{a})$. The $M \times N$ zero matrix is denoted as $\mathbf{0}_{M\times N}$.

B. BEAMFORMING FEEDBACK SCHEME IN IEEE 802.11ac/AX

We consider a MIMO communication system in which a transmitter (e.g., AP) transmits signals to the receiver (e.g., STA). We denote the CSI matrix from the transmitter to the receiver at the kth subcarrier as $\boldsymbol{H}_k \in \mathbb{C}^{M\times N}$, where M and N denote the number of antenna elements of the receiver and transmitter, respectively. In IEEE 802.11ac/ax standards, to provide efficient eigen beam-space division multiplexing [27], the receiver feeds back the BFF frame to the transmitter [4], [5], which contains a compressed version of the CSI matrix. Because the BFF frame is exchanged over the air without encryption, BFFs can be obtained using MAC frame-capturing tools, thus enabling an arbitrary sniffer to perform BFF-based WiFi sensing without requiring access to PHY layer components of the transmitter and receiver [7].

BFF contains the highly quantized right singular matrix $\boldsymbol{V}_k$ of the CSI matrix $\boldsymbol{H}_k$ for each subcarrier and a subcarrier-averaged stream gain [4], [5]. The right singular vector $\boldsymbol{V}_k$ is calculated using singular value decomposition as follows:

$$\boldsymbol{H}_k = \boldsymbol{U}_k \boldsymbol{\Sigma}_k {\boldsymbol{V}_k}^{\mathrm{H}}, \tag{1}$$

where $\boldsymbol{U}_k$ and $\boldsymbol{V}_k$ represent unitary matrices, and $\boldsymbol{\Sigma}_k$ denotes a diagonal matrix with singular values [28]. Denoting the number of subcarriers as K, the subcarrier-averaged stream gain is represented by a diagonal matrix $\bar{\boldsymbol{\Lambda}}$, where

$$\bar{\boldsymbol{\Lambda}} = \frac{1}{K}\sum_{k=1}^{K} {\boldsymbol{\Sigma}_k}^2. \tag{2}$$

Notably, the diagonal elements of $\boldsymbol{\Sigma}_k$ are generally real and positive and are listed in a descending order.

As per the IEEE 802.11ac/ax [4], [5] standards, $\boldsymbol{V}_k$ and $\bar{\boldsymbol{\Lambda}}$ are highly quantized to reduce the payload size of the BFF frame. Specifically, $\boldsymbol{V}_k$ is converted to N^{angle} angles without incurring any quantization losses using Givens rotation, where N^{angle} is determined by N and M. The N^{angle} angles are quantized using a predefined quantization step size Δ and are contained in a BFF frame. The IEEE 802.11ac standard [5] defines four quantization step sizes: $\pi/4$ rad, $\pi/8$ rad, $\pi/16$ rad, and $\pi/32$ rad. The subcarrier-averaged

stream gain $\bar{\boldsymbol{\Lambda}}$ is quantized with quantization step sizes of 0.25 dB [5].

C. PROPAGATION MODEL

We consider a discrete physical propagation model [26], in which a uniform linear array is employed at the transmitter and receiver. In the following description, for simplicity, we assume that the distances between consecutive antennas at the transmitter and receiver are the same and are denoted as d.[1]

Let L denote the number of propagation paths. Additionally, let ϕ_l be the AoD and θ_l be the angle of arrival of the lth path. The complex scalar r_l denotes attenuation from the transmitter's first antenna to the receiver's first antenna by the signal traveling along the lth propagation path. We denote a complex phase shift $a(\theta)$ as $\exp(2\pi d \sin(\theta)/\lambda)$, where λ represents the wavelength. For shorthand notation, let L-dimensional vectors $\boldsymbol{\theta}$, $\boldsymbol{\phi}$, and $\boldsymbol{r}$ represent $(\theta_1, \ldots, \theta_L)^{\mathrm{T}}$, $(\phi_1, \ldots, \phi_L)^{\mathrm{T}}$, and $(r_1, \ldots, r_L)^{\mathrm{T}}$, respectively. Additionally, we denote the steering vector $\boldsymbol{a}(\theta) := (1, a(\theta), \ldots, a(\theta)^{M-1})^{\mathrm{T}}$; $L \times M$ steering matrix $\boldsymbol{A}(\boldsymbol{\theta}) := (\boldsymbol{a}(\theta_1), \ldots, \boldsymbol{a}(\theta_L))^{\mathrm{T}}$; and $L \times L$ diagonal matrix $\boldsymbol{R} := \mathrm{diag}(\boldsymbol{r})$. In the discrete physical propagation model [26], the CSI matrix $\boldsymbol{H}$ is represented as follows:

$$\boldsymbol{H} = \boldsymbol{A}(\boldsymbol{\theta})\boldsymbol{R}\boldsymbol{A}(\boldsymbol{\phi})^{\mathrm{H}}. \tag{3}$$

D. MULTIPLE SIGNAL CLASSIFICATION (MUSIC) ALGORITHM

The CSI-based MUSIC algorithm [15] estimates multiple AoDs from CSI by assuming $L < N$. The general CSI-based MUSIC algorithm comprises the following three steps [14]–[16]: First, given an arbitrary slim and full-rank matrix $\boldsymbol{S}$, we estimate a matrix $\boldsymbol{X}$ represented by $\boldsymbol{S}\boldsymbol{A}(\boldsymbol{\phi})^{\mathrm{H}}$. For example, in [14], [16], the matrix $\boldsymbol{X}_0$ is a $K \times M$ matrix, whose kth row vector is the first row vector of the CSI matrix at the kth subcarrier.

Considering the propagation model denoted in (3), the first row vector of the CSI matrix at the kth subcarrier is represented by

$$\boldsymbol{h}_k = \left(\boldsymbol{r}_k^{\mathrm{T}}\boldsymbol{A}(\boldsymbol{\phi})^{\mathrm{H}}\right)^{\mathrm{T}}. \tag{4}$$

Given a $K \times L$ matrix $\boldsymbol{S}_0 := (\boldsymbol{r}_1, \ldots, \boldsymbol{r}_K)^{\mathrm{T}}$, the matrix $\boldsymbol{X}_0$ is represented by

$$\boldsymbol{X}_0 = (\boldsymbol{h}_1, \ldots, \boldsymbol{h}_1)^{\mathrm{T}} = \left(\boldsymbol{A}(\boldsymbol{\phi})^{*}\boldsymbol{r}_1, \ldots, \boldsymbol{A}(\boldsymbol{\phi})^{*}\boldsymbol{r}_K\right)^{\mathrm{T}} \tag{5}$$

$$= (\boldsymbol{r}_1, \ldots, \boldsymbol{r}_K)^{\mathrm{T}}\boldsymbol{A}(\boldsymbol{\phi})^{\mathrm{H}} = \boldsymbol{S}_0\boldsymbol{A}(\boldsymbol{\phi})^{\mathrm{H}}. \tag{6}$$

Generally, $\boldsymbol{S}_0$ is slim and full-rank [15], [16]; thus, $\boldsymbol{X}_0$ is represented as a product of the slim and full-rank matrix and $\boldsymbol{A}(\boldsymbol{\phi})^{\mathrm{H}}$.

Second, a covariance matrix $\boldsymbol{C} := \boldsymbol{X}^{\mathrm{H}}\boldsymbol{X}$ is obtained, and $M - L$ noise subspace vectors $\boldsymbol{e}_1, \ldots, \boldsymbol{e}_{M-L}$ are calculated as $M - L$ eigenvectors of $\boldsymbol{C}$ with small eigenvalues. Lastly, the AoDs are estimated as angles that achieve peaks of the MUSIC spectrum $g(\phi)$, where

$$g(\phi) := \frac{1}{\boldsymbol{a}(\phi)^{\mathrm{H}}\boldsymbol{E}_{\mathrm{N}}{}^{\mathrm{H}}\boldsymbol{E}_{\mathrm{N}}\,\boldsymbol{a}(\phi)}, \tag{7}$$

where $\boldsymbol{E}_{\mathrm{N}} = (\boldsymbol{e}_1, \ldots, \boldsymbol{e}_{M-L})$.

[1]This assumption can be easily expanded to the case in which the distances between consecutive antennas differ between the transmitter and receiver.

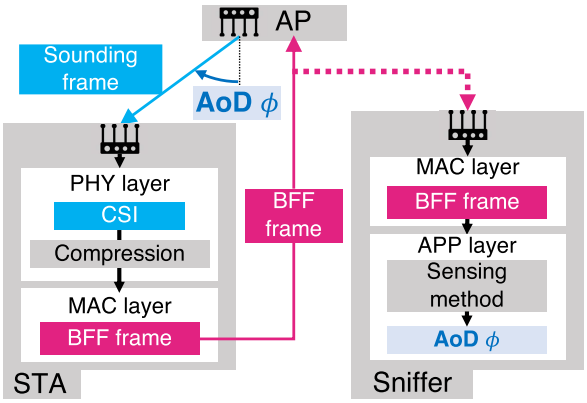

FIGURE 1. System model of BFF-based MUSIC. STA transmits BFF to AP without encryption, allowing the sniffer to capture the BFF and conduct BFF-based sensing.

IV. BEAMFORMING FEEDBACK-BASED MULTIPLE SIGNAL CLASSIFICATION

Fig. 1 illustrates the system model comprising an STA, an AP, and a sniffer. The STA receives the sounding frame (e.g., the null data packet in IEEE 802.11ac/ax [4], [5]) from the AP, estimates the CSI, and calculates the BFF from the CSI, which is detailed in Section III-B. Then, the STA transmits the BFF to the AP without any encryption. The sniffer captures the BFF transmitted from the STA, decodes the BFF, and obtains the right singular matrix $\boldsymbol{V}_k$ for each subcarrier and subcarrier-averaged stream gain $\bar{\boldsymbol{\Lambda}}$. Subsequently, the sniffer estimates the AoDs of the AP using the BFF-based MUSIC algorithm, which is detailed in the following sections.

We confirmed that the MUSIC algorithm is applicable for using the BFF to estimate multiple AoDs, which has been proven in Proposition 1. Specifically, assuming $\bar{\boldsymbol{\Lambda}} = \boldsymbol{\Sigma}_k{}^2$ for all k, the covariance matrix used in the MUSIC algorithm can be estimated as follows:

$$\boldsymbol{C} = \sum_{k=1}^{K} \boldsymbol{V}_k \bar{\boldsymbol{\Lambda}}\, \boldsymbol{V}_k{}^{\mathrm{H}}. \tag{8}$$

Based on the covariance matrix,[2] the AoDs are estimated by the general MUSIC algorithm, which is detailed in Section III-D.

[2]It should be noted that in [11], (8) was used for the feature extraction method in the data preprocessing procedure for data-driven BFF-based sensing.

Theorem 1: Given a slim and full-rank matrix $\boldsymbol{S}$ and assuming $\bar{\boldsymbol{\Lambda}} = \boldsymbol{\Sigma}_k{}^2$, the covariance matrix $\boldsymbol{C}$ defined in (8) is denoted by the covariance matrix of $\boldsymbol{S}\boldsymbol{A}(\boldsymbol{\phi})^{\mathrm{H}}$.

Proof: Based on the aforementioned assumptions, $\boldsymbol{C}$ in (8) is expressed as follows:

$$\boldsymbol{C} = \sum_{k=1}^{K} \boldsymbol{V}_k \boldsymbol{\Sigma}_k{}^2 \boldsymbol{V}_k{}^{\mathrm{H}}. \tag{9}$$

Substituting (1) and (3) into $\boldsymbol{C}$, we obtain

$$\begin{aligned}\boldsymbol{C} &= \sum_{k=1}^{K} \boldsymbol{H}_k{}^{\mathrm{H}} \boldsymbol{H}_k = \sum_{k=1}^{K} \boldsymbol{A}(\boldsymbol{\phi}) \boldsymbol{R}_k{}^{\mathrm{H}} \boldsymbol{A}(\boldsymbol{\theta}) \boldsymbol{A}(\boldsymbol{\theta})^{\mathrm{H}} \boldsymbol{R}_k \boldsymbol{A}(\boldsymbol{\phi})^{\mathrm{H}} \\ &= \boldsymbol{A}(\boldsymbol{\phi}) \left(\sum_{k=1}^{K} \boldsymbol{R}_k{}^{\mathrm{H}} \boldsymbol{A}(\boldsymbol{\theta}) \boldsymbol{A}(\boldsymbol{\theta})^{\mathrm{H}} \boldsymbol{R}_k \right) \boldsymbol{A}(\boldsymbol{\phi})^{\mathrm{H}}. \end{aligned} \tag{10}$$

Using $KM \times M$ matrix $\boldsymbol{S} := \left(\boldsymbol{R}_1{}^{\mathrm{H}} \boldsymbol{A}(\boldsymbol{\theta}), \ldots, \boldsymbol{R}_K{}^{\mathrm{H}} \boldsymbol{A}(\boldsymbol{\theta}) \right)^{\mathrm{H}}$,

$$\boldsymbol{C} = \boldsymbol{A}(\boldsymbol{\phi}) \boldsymbol{S}^{\mathrm{H}} \boldsymbol{S} \boldsymbol{A}(\boldsymbol{\phi})^{\mathrm{H}}. \tag{11}$$

Thus, this proposition proves that $\boldsymbol{S}$ is a full-rank matrix. Based on the deduction that $\boldsymbol{S}_0$ is slim and full-rank, which is detailed in Section III-D, the above proposition can be proven by an indirect proof. We denote a diagonal matrix $\hat{\boldsymbol{A}}(\boldsymbol{\theta})$ as $\mathrm{diag}(a(\theta_1), \ldots, a(\theta_L))$. If $\boldsymbol{S}$ is not a full-rank matrix, a non-zero vector $\boldsymbol{x} \in \mathbb{C}^L$ satisfies

$$\boldsymbol{S}\boldsymbol{x} = \boldsymbol{0}_{KM \times 1}. \tag{12}$$

The equation (12) is equivalent to

$$\boldsymbol{S}_0 \hat{\boldsymbol{A}}(\boldsymbol{\theta})^{m-1} \boldsymbol{x} = \boldsymbol{0}_{K \times 1}, \ \forall m = 1, \ldots, M. \tag{13}$$

However, as denoted in [14], $\boldsymbol{S}_0$ is generally a slim and full-rank matrix, and $\hat{\boldsymbol{A}}(\boldsymbol{\theta})^{m-1}$ is regular; thus, this presents a contradiction. □

A. DETAILED PROCEDURE

The detailed procedure of the BFF-based MUSIC algorithm is presented in Algorithm 1. The STA estimates the CSI using a sounding frame transmitted from the AP, calculates the BFF from the CSI, and transmits the BFF to the AP. We denote $\boldsymbol{H}_{k,i}$ as the CSI matrix at the kth subcarrier from the ith sounding frame. We also denote the right singular matrix and subcarrier-averaged stream gain of $\boldsymbol{H}_{k,i}$ as $\boldsymbol{V}_{k,i}$ and $\bar{\boldsymbol{\Lambda}}_i$, respectively. The BFF corresponding to the ith sounding frame includes $\left(\boldsymbol{V}_{1,i}, \ldots, \boldsymbol{V}_{K,i} \right)$ and $\bar{\boldsymbol{\Lambda}}_i$. $\bar{\boldsymbol{\Lambda}}_i$ and $\boldsymbol{V}_{k,i}$ include quantization errors because the BFF frame is highly quantized in IEEE 802.11ac/ax [4], [5], which is detailed in Section III-B.

The frame capture obtains N^{pct} BFF frames transmitted from the STA and can estimate multiple AoDs of the AP from the BFF frames. For each captured BFF frame, the frame capture obtains the subcarrier-averaged stream gain $\bar{\boldsymbol{\Lambda}}_i$ and the right singular matrix $\boldsymbol{V}_{k,i}$. Using $\bar{\boldsymbol{\Lambda}}_i$ and $\boldsymbol{V}_{k,i}$, the covariance matrix $\boldsymbol{C}_i$ is calculated as follows:

$$\boldsymbol{C}_i = \frac{1}{K} \sum_{k=1}^{K} \boldsymbol{W}_k \boldsymbol{V}_{k,i} \bar{\boldsymbol{\Lambda}}_i \boldsymbol{V}_{k,i}{}^{\mathrm{H}} \boldsymbol{W}_k^{\mathrm{H}}, \tag{14}$$

Algorithm 1 BFF-Based MUSIC

Input: N^{pct} BFF frames

1: **for** each packet i **do**
2: $\quad \boldsymbol{C}_i = \frac{1}{K} \sum_{k=1}^{K} \boldsymbol{W}_k \boldsymbol{V}_{k,i} \bar{\boldsymbol{\Lambda}}_i \boldsymbol{V}_{k,i}{}^{\mathrm{H}} \boldsymbol{W}_k^{\mathrm{H}}$.
3: **end for**
4: Averaging among packets: $\boldsymbol{C}^{\mathrm{ave}} = \frac{1}{N^{\mathrm{pct}}} \sum_{n=1}^{N^{\mathrm{pct}}} \boldsymbol{C}_n$
5: Spatial smoothing: $\boldsymbol{C}^{\mathrm{smt}} = f^{\mathrm{smt}}(\boldsymbol{C}^{\mathrm{ave}})$
6: Obtain eigenvectors $\boldsymbol{e}_1, \ldots, \boldsymbol{e}_M$ of $\boldsymbol{C}^{\mathrm{smt}}$, where $\boldsymbol{e}_1, \ldots, \boldsymbol{e}_M$ is aligned in descending order of its eigenvalue.
7: Calculate the noise subspace matrix $\boldsymbol{E}_{\mathrm{N}} = (\boldsymbol{e}_1, \ldots, \boldsymbol{e}_{M-L})^{\mathrm{T}}$.
8: Evaluate the MUSIC spectrum $1/\boldsymbol{a}(\phi)^{\mathrm{H}} \boldsymbol{E}_{\mathrm{N}}{}^{\mathrm{H}} \boldsymbol{E}_{\mathrm{N}} \boldsymbol{a}(\phi)$.
9: Obtain AoDs as L peaks of the MUSIC spectrum.

where $\boldsymbol{W}_k$ denotes a diagonal matrix that compensates for the phase shift introduced at the AP. The methods employed to estimate $\boldsymbol{W}_k$ are detailed in Section IV-B. We average $\boldsymbol{C}_i$ among N^{pct} packets and use the averaged covariance matrix $\boldsymbol{C}^{\mathrm{ave}}$ in the following MUSIC procedure, where

$$\boldsymbol{C}^{\mathrm{ave}} = \frac{1}{N^{\mathrm{pct}}} \sum_{i=1}^{N^{\mathrm{pct}}} \boldsymbol{C}_i. \tag{15}$$

Following the existing CSI-based MUSIC methods [15], [29], we apply spatial smoothing to $\boldsymbol{C}^{\mathrm{ave}}$. We denote the spatial smoothing function as f^{smt} and the smoothed covariance matrix as $\boldsymbol{C}^{\mathrm{smt}}$, where $\boldsymbol{C}^{\mathrm{smt}} = f^{\mathrm{smt}}(\boldsymbol{C}^{\mathrm{ave}})$. The spatial smoothing procedure is detailed in Section IV-C. From the smoothed covariance matrix $\boldsymbol{C}^{\mathrm{smt}}$, we estimate the AoDs using the general MUSIC algorithm [16], as described in Section III-D.

Notably, estimation of the number of propagation paths L is required in the BFF-based MUSIC algorithm as in the CSI-based MUSIC algorithm. In this work, we assume that L is given, and the number of path estimation problem lies outside the scope of this study. This is because the problem is not specific to BFF-based sensing.

B. CALIBRATION PROCEDURE

To perform accurate AoD estimation, the compensation for the phase offset introduced at the AP is required [15]. To this end, we implemented a calibration method that estimates the phase shift difference between the antenna elements. The calibration procedure measures the BFF in the environment where the number of propagation paths is only one, and the AoD is given; subsequently, the phase offset at the AP is estimated. Specifically, the calibration procedure is as follows: the covariance matrix of the CSI matrix is estimated from the BFF, and the eigenvector of the covariance matrix with the largest eigenvalue corresponds to the phase shift of the AP.

Formally, we denote the phase offset introduced at the nth antenna of the AP as $\mathrm{e}^{\mathrm{j}\tau_{n,k}}$. The calibration procedure then estimates $\mathrm{e}^{\mathrm{j}(\tau_{n,k} - \tau_{1,k})}$. For a shorthand notation, we denote a diagonal matrix $\boldsymbol{W}_k$ as $\mathrm{diag}\left(1, \mathrm{e}^{\mathrm{j}(\tau_{2,k} - \tau_{1,k})}, \ldots, \mathrm{e}^{\mathrm{j}(\tau_{N,k} - \tau_{1,k})}\right)$.

Considering the $N \times 1$ MIMO system, and given that $L = 1$ and the pre-obtained AoD is $\hat{\phi}$, the observed CSI matrix is denoted as follows:

$$\boldsymbol{H}_k^{\mathrm{obs}} = \mathrm{e}^{\mathrm{j}\tau_{1,k}} r_k \boldsymbol{a}(\hat{\phi})\, \boldsymbol{W}_k, \tag{16}$$

where r_k denotes the complex path gain.

The calibration procedure estimates $\boldsymbol{W}_k$ using the pre-obtained AoD $\hat{\phi}$ and BFF calculated from $\boldsymbol{H}_k^{\mathrm{obs}}$ as follows. We denote the right singular matrix and subcarrier-averaged stream gain of $\boldsymbol{H}_k^{\mathrm{obs}}$ as $\boldsymbol{V}_k^{\mathrm{obs}}$ and $\bar{\boldsymbol{\Lambda}}^{\mathrm{obs}}$, respectively. First, the covariance matrix of $\boldsymbol{H}_k^{\mathrm{obs}}$ is estimated as $\boldsymbol{V}_k^{\mathrm{obs}} \bar{\boldsymbol{\Lambda}}^{\mathrm{obs}} (\boldsymbol{V}_k^{\mathrm{obs}})^{\mathrm{H}}$. The covariance matrix is also represented as follows:

$$(\boldsymbol{H}_k^{\mathrm{obs}})^{\mathrm{H}} \boldsymbol{H}_k^{\mathrm{obs}} = |r_k|^2 \boldsymbol{W}_k{}^{\mathrm{H}} \boldsymbol{a}(\hat{\phi})^{\mathrm{H}} \boldsymbol{a}(\hat{\phi})\, \boldsymbol{W}_k. \tag{17}$$

From (17), the covariance matrix has $N-1$ eigenvectors with an eigenvalue of zero and an eigenvector with an eigenvalue of $|r_k|^2$, and the latter eigenvector is $\boldsymbol{W}_k{}^{\mathrm{H}} \boldsymbol{a}(\hat{\phi})^{\mathrm{H}}$. Thus, denoting the latter eigenvector as $\boldsymbol{x} := (1, x_2, \ldots, x_N)^{\mathrm{T}}$, $\boldsymbol{W}_k$ is estimated as

$$\boldsymbol{W}_k = \mathrm{diag}(\boldsymbol{a}(\hat{\phi}))^{\mathrm{H}} \mathrm{diag}(\boldsymbol{x})^{\mathrm{H}}. \tag{18}$$

In the MUSIC algorithm, which is implemented after calibration, $\boldsymbol{W}_k \boldsymbol{V}_k$ is used instead of $\boldsymbol{V}_k$.

C. SPATIAL SMOOTHING

As described in [15], [29], when multipath signals are phase-synchronized with each other, distinct multipath signals are recognized as one superposed signal, resulting in false peaks in the MUSIC spectrum. To address this problem, we adopt spatial smoothing [15], [29], which splits the antenna array of an AP into multiple sub-antenna arrays. Given that M' antennas are integrated into a sub-antenna array, the antenna array with M antennas is considered as $M - M' + 1$ sub-antenna arrays. The covariance matrix is calculated for each sub-antenna array in the spatial smoothing procedure, and the covariance matrices are averaged. Specifically, given the covariance matrix for the jth sub-antenna array as $\boldsymbol{C}_j^{\mathrm{sub}} \in \mathbb{C}^{M' \times M'}$, $\boldsymbol{C}_j^{\mathrm{sub}}$ is a submatrix of $\boldsymbol{C}$, where $1, \ldots, j-1$, $j+M', \ldots, M$ rows and columns are removed from $\boldsymbol{C}$. The averaged covariance matrix $\boldsymbol{C}^{\mathrm{smt}} \in \mathcal{C}^{M' \times M'}$ is obtained as follows:

$$\boldsymbol{C}^{\mathrm{smt}} = \frac{1}{M - M' + 1} \sum_{j=1}^{M-M'+1} \boldsymbol{C}_j^{\mathrm{sub}}. \tag{19}$$

The averaged covariance matrix $\boldsymbol{C}^{\mathrm{smt}}$ is used for estimating the noise subspace vectors, instead of the original covariance matrix $\boldsymbol{C}$.

V. NUMERICAL EVALUATION

Because ground-truth multiple AoDs generally cannot be measured in a real-world environment, we examined the capacity of BFF-based MUSIC to estimate multiple AoDs through numerical evaluations. Moreover, in the extensive experimental evaluations in real-world environments presented in Section VI, we evaluated the accuracy of AoD estimation, assuming that only the direct path exists.

A. SETUP

Fig. 2 illustrates the system, which comprises an AP, an STA, and a reflection point, resulting in two different propagation paths between an antenna element of the AP and that of the STA—i.e., a direct path and an indirect path caused by the reflection point. The STA and reflection point exist at (0 m, 10 m) and (5.5 m, 3 m), respectively, whereas the AP exists at any of the 11 points along the x-axis. Specifically, the n_{a}th position of the AP is denoted by $(n_{\mathrm{a}} - 5\,\mathrm{m}, 0\,\mathrm{m})$, where $0 \le n_{\mathrm{a}} \le 10$. The AP and STA are equipped with uniform array antennas. Each of the antenna arrays contains four antenna elements that are parallel to the x-axis.

We assume free-space propagation, wherein indirect paths are decayed by a factor of 0.3 in amplitude, and we ignore the effect of reflection more than once. CSI estimation is emulated by adding Gaussian noise to the ground-truth CSI matrix $\boldsymbol{H}_k$. Specifically, the estimated CSI at the kth subcarrier is denoted as follows:

$$\boldsymbol{H}_k^{\mathrm{obs}} = \boldsymbol{H}_k + \boldsymbol{N}, \tag{20}$$

where $\boldsymbol{N}$ represents an $M \times N$ complex matrix, for which real and imaginary parts of the elements follow a Gaussian distribution with a mean of zero and a variance of $\sigma^2/2$. Note that σ^2 denotes the noise power at each antenna element. We calculate $\boldsymbol{H}_k^{\mathrm{obs}}$ for each subcarrier k and then obtain $\boldsymbol{V}_k$ for each subcarrier and subcarrier-averaged stream gain $\bar{\boldsymbol{\Lambda}}$ by following the procedure detailed in Section III-B. Specifically, we select the quantization step size Δ of $\pi/32$ rad for quantization of $\boldsymbol{V}_k$,[3] leading to a representation of the 4×4 right singular matrix $\boldsymbol{V}_k$ by only 60 bit. Additionally, as defined in the IEEE 802.11ac [5], the subcarrier-averaged stream gain $\bar{\boldsymbol{\Lambda}}$ is quantized with a quantization step size of 0.25 dB.

Moreover, to assess the error involved in multiple AoD estimations, we swap the order of the estimated AoDs to minimize the error between the estimated AoDs and ground-truth AoDs; subsequently, the error is calculated from the swapped versions of the estimated and ground-truth AoDs. The detailed parameters are as follows: the distance of each antenna element is 25 mm, number of subcarriers is 52, bandwidth is 20 MHz, center frequency is 5.18 GHz, number of CSIs used for each AoD estimation N^{pct} is 10, and number of antenna elements in each sub-antenna array M' is two.

B. RESULT

Fig. 3 presents an example of the MUSIC spectrum function $g(\phi)$ of the BFF- and CSI-based MUSIC algorithms, respectively. The results presented in Fig. 3 are obtained under the setting that the signal-to-noise ratio (SNR) is 20 dB, and the AP exists at $(-3\,\mathrm{m}, 0\,\mathrm{m})$, which denotes the AP position surrounded by the red square in Fig. 2. The two peaks of the MUSIC spectrum function indicate the two estimated AoDs.

[3]The quantization step size Δ of $\pi/32$ rad is one of the quantization step sizes defined in IEEE 802.11ac and is used in the BFF procedure in commercial APs, ASUS RT-AC86U and Buffalo WXR-5700AX7S.

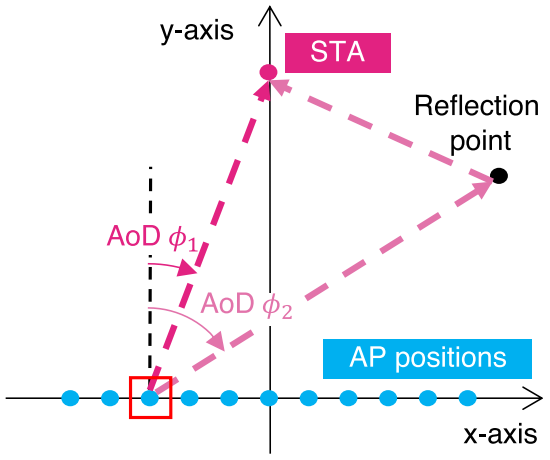

FIGURE 2. Numerical evaluation environment. The STA and reflection point exist at (0 m, 10 m) and (5.5 m, 3 m) in a two-dimensional space, respectively. The AP exists at either of the 11 points denoted by blue dots. Color-dotted lines indicate two propagation paths when the AP exists on a point surrounded by a red square.

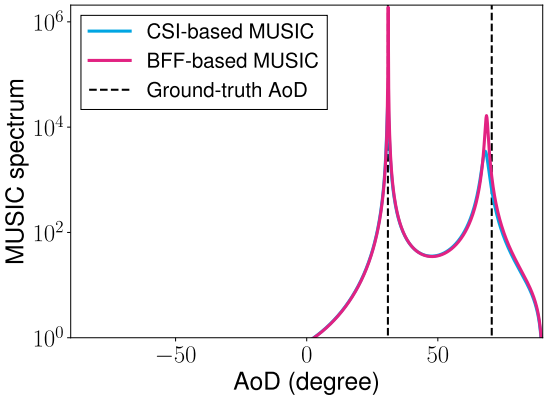

FIGURE 3. MUSIC spectrum function of BFF- and CSI-based MUSIC obtained through numerical evaluation. The two peaks of the function indicate the two estimated AoDs.

The estimated AoDs of the BFF-based MUSIC match with the ground-truth AoDs, as well as with that of the CSI-based MUSIC.

Table 2 lists the median of the absolute error of the AoD estimation performed using CSI- and BFF-based MUSIC for each SNR. Regardless of the SNR, the error resulting from CSI-based MUSIC is lower than or equal to that resulting from BFF-based MUSIC. This is because BFF is highly quantized; specifically, the 4×4 right singular matrix is represented by only 60 bit. However, the difference in the error between the two sensing methods is trivial. Specifically, for estimation of the AoDs for the direct and indirect paths, the difference is smaller than 0.03° and 0.4°, respectively. Thus, we can conclude that BFF-based MUSIC accurately estimates multiple AoDs; moreover, the accuracy of BFF-based MUSIC is comparable to that of CSI-based MUSIC. If the BFF is not quantized, the result of AoD estimation by the CSI and BFF matches perfectly.

TABLE 2. Median of the absolute error of AoD estimation by CSI- and BFF-based MUSIC for each SNR.

SNR	CSI		BFF	
	Direction path	indirection path	Direction path	indirection path
5 dB	0.11°	2.4°	0.13°	2.8°
10 dB	0.09°	1.0°	0.09°	1.1°
20 dB	0.06°	0.2°	0.09°	0.3°

VI. EXPERIMENTAL EVALUATION

This study evaluated the accuracy of the BFF- and CSI-based MUSIC algorithms in various real-world environments, where a line-of-sight (LoS) path between the AP and STA exists. Notably, this evaluation is based on the assumption that the number of propagation paths is one (i.e., only the direct path exists), and the ground-truth AoD is defined as the AoD of the LoS path. This assumption is adopted because we cannot measure the ground-truth AoDs of the reflection paths in real-world environment.

Experimental evaluations were performed in three real-world scenarios: indoor, outdoor, and semi-outdoor. The indoor, outdoor, and semi-outdoor scenarios differ in terms of the effect of reflection paths. Specifically, the received power caused by the reflection paths in the indoor scenario is generally larger than that caused by the reflection paths in the outdoor and semi-outdoor scenarios. The outdoor and semi-outdoor scenarios differ in terms of the method used for varying the AoD. In the outdoor scenario, the position and orientation of the antenna array of the AP are fixed, and the AoD only depends on the position of the STA. However, in the semi-outdoor scenario, the AP and STA are fixed, and the AoD only depends on the orientation of the AP's antenna array.

A. SETUP

1) EXPERIMENTAL EQUIPMENT

The experimental system comprises an AP and STA equipped with three and two antennas, respectively, resulting in the 2×3 CSI matrix. As shown in Fig. 4, the antenna elements of the AP are linearly aligned, where the distance between conservative antenna elements is 25 mm. The communication protocol, wireless channel, bandwidth, and number of subcarriers are IEEE 802.11ac, 104ch, 20 MHz, and 52, respectively. Moreover, ASUS RT-AC86U is used for the AP and STA. The detailed parameters of the MUSIC algorithm are as follows: the number of CSIs or BFFs used for each AoD estimation N^{pct} is 10, and the number of antenna elements in each sub-antenna array M' is two.

2) BFF ESTIMATION

Notably, for a fair comparison between CSI- and BFF-based sensing, we used a firmware modification [23] to extract CSI from the AP and calculate BFF from the extracted CSI. Specifically, assuming channel reciprocity, we emulated the CSI measured at the STA as the transpose of the

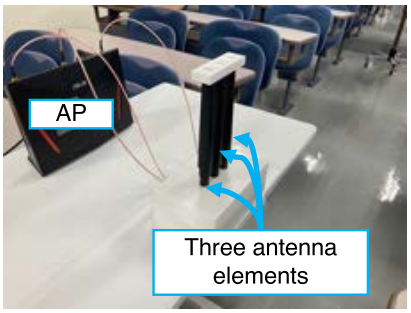

FIGURE 4. Snapshot of AP. Three antennas are linearly aligned with 25 mm of space between the antennas.

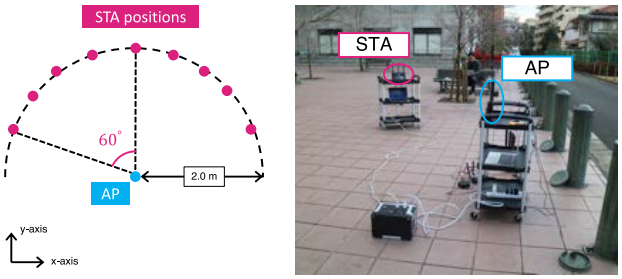

(a) Equipment layout. (b) Snapshot.

FIGURE 5. Outdoor experimental scenario. STA is placed at any of the nine red points. AP and STA are located at a height of 0.9 m.

CSI measured at the AP. From the CSI, the corresponding BFF was calculated following the IEEE 802.11ac standard, as described in Section III-B.

Because the shape of the CSI is 2×3, the right singular matrix $\boldsymbol{V}_k$ is represented by 12 angles with a quantization step size of Δ. Unless otherwise noted, this evaluation uses Δ of $\pi/32$ rad, resulting in a 2×3 complex matrix $\boldsymbol{V}_k{}^{\mathrm{H}}$ represented by 30 bit.[3] Additionally, as defined in the IEEE 802.11ac standard [5], the subcarrier-averaged stream gain $\bar{\boldsymbol{\Lambda}}$ is quantized with a quantization width of 0.25 dB.

3) EXPERIMENTAL SCENARIO

The experimental evaluation was performed under three scenarios: outdoor, semi-outdoor, and indoor. An LoS path exists between the AP and STA in all three scenarios. For all the scenarios, the CSIs and corresponding BFFs were obtained for multiple arrangements of the AP and STA, where the ground-truth AoD differed based on the arrangement. Regardless of the scenario, the AP captures approximately 850 packets from the STA for each equipment arrangement and estimates the CSI and BFF for each captured packet.

Fig. 5 presents the setup and snapshot of the outdoor scenario. The STA is placed at any of the nine positions on the circle with a radius of 2.0 m, centered on the AP. The orientations of the antenna array of the AP and STA are fixed to be parallel to the x-axis. Thus, the AoD only depends on the position of the STA, resulting in the AoD lying in a range of $-60°$ to $60°$ in $15°$ increments.

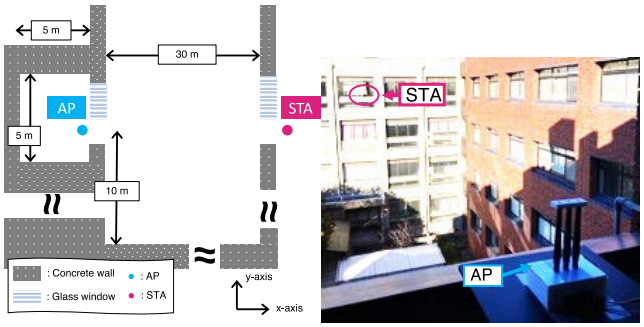

(a) Setup. (b) Snapshot.

FIGURE 6. Semi-outdoor experimental scenario. AP and STA are located in different rooms on the fourth floor, where the LoS path exists through open windows. The height of AP and STA from the floor is 0.9 m and that of the rooms is 3.0 m.

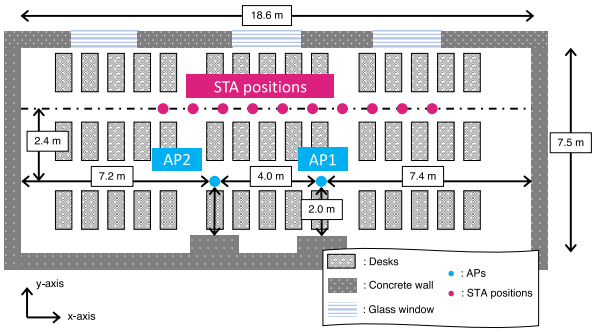

(a) Setup.

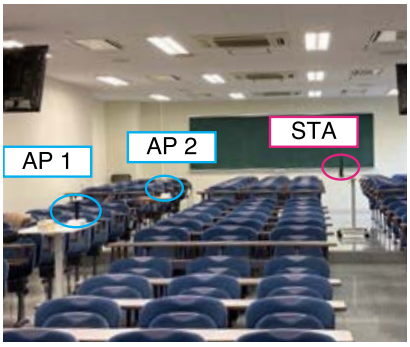

(b) Snapshot.

FIGURE 7. Indoor experimental scenario. STA is placed at any of the 10 red points, whereas two APs are located at the blue points. The heights of the AP and STA are 0.9 m. The height, width, and depth of the room are 3.0 m, 7.5 m, and 18.6 m, respectively.

Fig. 6 presents the semi-outdoor experimental scenario and its snapshot. The AP and STA are fixed in different rooms, where the LoS exists through open windows. In the semi-outdoor environment, the orientation of the antenna array of the AP is changed, whereas the orientation of the antenna array of the STA is fixed parallel to the y-axis. Thus, the AoD only depends on the orientation of the antenna array of the AP.

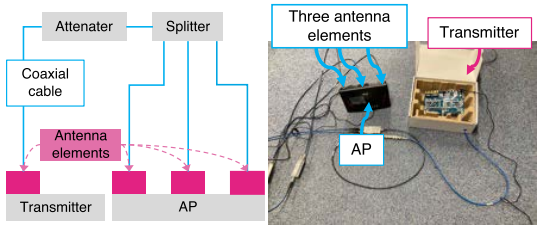

(a) Wiring diagram. (b) Snapshot.

FIGURE 8. Setup of the calibration procedure. The lengths of the coaxial cables are adjusted so that phases at the three antennas of the AP are the same.

Specifically, the orientation of the AP is changed so that the AoD lies in the range of $-60°$ to $60°$ in $15°$ increments.

Fig. 7 presents the indoor experimental scenario and its snapshot. The two APs and STA are located in a lecture room, where the orientation of the antenna array of the APs and STA is fixed parallel to the y-axis. While the APs are fixed, the STA is located at any of the 10 positions along a line parallel to the x-axis, where the distance between the line and AP is 2.4 m. Thus, the AoD only depends on the position of the STA. In this scenario, the AoD is varied from approximately $-60°$ to $60°$. It should be noted that AoD estimation is conducted for each AP.

4) CALIBRATION PROCEDURE

Fig. 8 illustrates the setup of the calibration procedure. The AP's antennas and a transmitter antenna are connected via coaxial cables. Because the length of coaxial cables between the antenna of the AP and the transmitter remains the same among the three antennas of the AP, the phases of the antennas of AP are considered to be the same, and there exists only a direct wave (i.e., $L = 1$ and $\hat{\phi} = 0$). We captured approximately 1,000 packets in the environment, obtained CSIs, and calculated BFFs. From the BFFs, we estimated the calibration matrix $\boldsymbol{W}$, as detailed in Section IV-B.

B. RESULTS

1) RESULTS OF THE CALIBRATION PROCEDURE

Fig. 9 depicts the angle of the estimated calibration matrix $\boldsymbol{W}_k$ from the BFF with quantization step sizes of $\pi/32$ rad and $\pi/4$ rad, and CSI, respectively. As detailed in Section IV-B, the calibration matrix $\boldsymbol{W}_k$ is denoted as $\mathrm{diag}(1, W_{k,2}, W_{k,3})$. Thus, Fig. 9 depicts the argument of $W_{k,2}$ and $W_{k,3}$. When the quantization step size is $\pi/32$ rad, the estimated arguments from the BFF match those from the CSI; specifically, the difference between the arguments estimated from the BFF and CSI is smaller than $2.3°$ regardless of the subcarrier index. Thus, we can conclude that when the quantization step size is small, the results of the BFF-based calibration accurately match those of the CSI-based calibration.

As the quantization step size is increased, the difference in the estimated arguments between the BFF and CSI increases owing to the quantization error induced in the BFF. Specifically, when the quantization step size is $\pi/4$ rad, the median and maximum difference between the estimated arguments from the BFF and CSI are $15.4°$ and $25.0°$, respectively. However, the following evaluations reveal that, even when the quantization step size is large, the AoD estimation accuracy of BFF-based MUSIC is comparable to that of the CSI-based method.

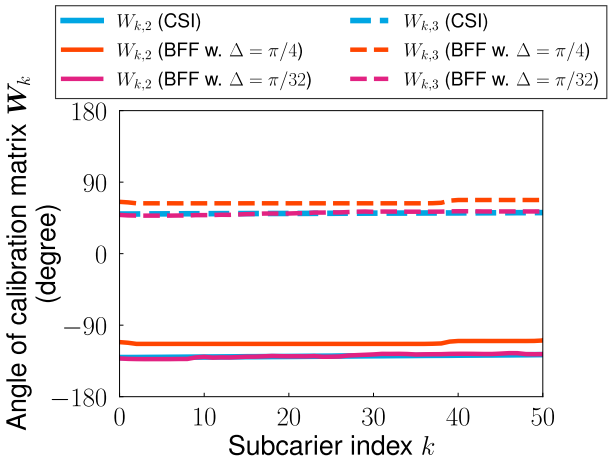

FIGURE 9. Angle of the estimated calibration matrix $\boldsymbol{W}_k$ from BFF and CSI, respectively. Calibration matrix $\boldsymbol{W}_k$ is represented by $\mathrm{diag}(1, \boldsymbol{W}_{k,2}, \boldsymbol{W}_{k,3})$.

TABLE 3. Median of the absolute error of AoD estimation by CSI- and BFF-based MUSIC for each scenario.

Scenario	CSI	BFF
Outdoor	10.3°	10.3°
Semi-outdoor	10.2°	9.8°
Indoor w. AP1	17.9°	17.1°
Indoor w. AP2	14.7°	14.8°

2) AoD ESTIMATION ERROR COMPARISON

Fig. 10 illustrates the empirical cumulative distribution function (CDF) of the AoD estimation error resulting from BFF- and CSI-based MUSIC. In Fig. 10, the error resulting from BFF-based MUSIC is comparable to that resulting from CSI-based MUSIC, regardless of the experimental scenario. Table 3 lists the error medians of AoD estimation by CSI-based MUSIC and BFF-based MUSIC in the three scenarios. As shown in Fig. 10, regardless of the scenario, the errors resulting from BFF- and CSI-based MUSIC are comparable. Thus, the AoD estimation accuracy of BFF-based MUSIC is comparable to that of CSI-based MUSIC, although BFF is highly quantized; specifically, the 2×3 right singular matrix is represented by only 30 bit, and the subcarrier-averaged stream gain is represented with a quantization step size of 0.25 dB.

Additionally, the error resulting from CSI-based MUSIC in this evaluation is comparable to the previously reported value [19], that is approximately $10°$. Although the error associated with AoD estimation largely depends on the experimental environment and the equipment used (e.g., the antenna

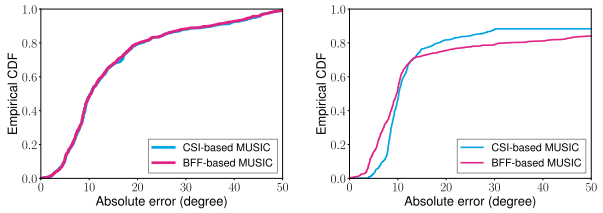

(a) Outdoor scenario. (b) Semi-outdoor scenario.

(c) Indoor scenario w. AP1. (d) Indoor scenario w. AP2.

FIGURE 10. Empirical CDF of the absolute error of AoD estimation by CSI-based MUSIC and BFF-based MUSIC for each scenario.

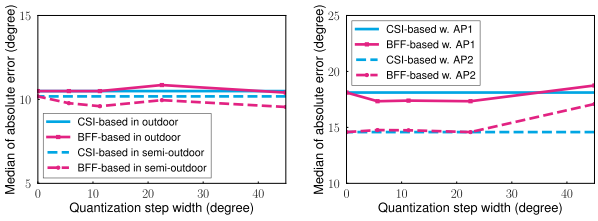

(a) Outdoor and semi-outdoor scenario. (b) Indoor scenario.

FIGURE 11. Impact of quantization step size on the median error of AoD estimation for each scenario.

characteristics, propagation environment, placement of the AP and STA, assumption that the number of propagation paths is one, and performance of calibration), the similarity of error between the one reported in this paper and that in an existing report [19] indicates that the implementation in this study is adequate. Note that developing methods that are agnostic to these experimental environments and equipment is a future challenge.

Upon comparing the estimation errors between the scenarios, the errors for indoor scenarios were found to be higher than those for outdoor and semi-outdoor scenarios for both CSI- and BFF-based MUSIC. This is because the number of propagation paths in the indoor scenario is larger than that in the outdoor and semi-outdoor scenarios. Furthermore, because we assumed $L = 1$ in this experimental evaluation, the larger multipath degrades the accuracy of AoD estimation.

3) IMPACT OF QUANTIZATION STEP SIZE

Fig. 11 presents the impact of the quantization step size on the AoD estimation error resulting from BFF-based MUSIC. In IEEE 802.11ac [5], four quantization step sizes Δ of $\boldsymbol{V}_k$ are defined: $\pi/4$ rad, $\pi/8$ rad, $\pi/16$ rad, and $\pi/32$ rad. Regardless of the experimental scenario, the impact of the quantization step size on the median of error is less than 3.0°. Moreover, regardless of the experimental scenario and the quantization step size, the AoD estimation error of BFF-based MUSIC is comparable to that of the CSI-based methods. Thus, even when the AP adopts the largest quantization step size defined in IEEE 802.11ac, the AoD estimation accuracy of BFF-based MUSIC is comparable to that of CSI-based MUSIC.

VII. CONCLUSION

This study confirmed that, to estimate multiple AoDs, an extension of the MUSIC algorithm is applicable using BFF, which contains only subcarrier-averaged stream gain and the highly quantized right singular matrix. Numerical and experimental evaluations on three scenarios revealed that the AoD estimation accuracy of BFF-based MUSIC is comparable to that of CSI-based MUSIC.

REFERENCES

[1] Y. Ma, G. Zhou, and S. Wang, "WiFi sensing with channel state information: A survey," *ACM Comput. Surv.*, vol. 52, no. 3, pp. 1–36, Jan. 2019.
[2] F. Zafari, A. Gkelias, and K. K. Leung, "A survey of indoor localization systems and technologies," *IEEE Commun. Surveys Tuts.*, vol. 21, no. 3, pp. 2568–2599, Apr. 2019.
[3] *Wireless LAN Medium Access Control (MAC) and Physical Layer PHY) Specifications Amendment: Enhancements for WLAN Sensing*, Standard P802.11bf, 2020.
[4] *Wireless LAN Medium Access Control (MAC) and Physical Layer (PHY) Specifications Amendment 1: Enhancements for High-Efficiency WLAN*, Standard IEEE Std. 802.11ax-2021, May 2021.
[5] *Wireless LAN Medium Access Control (MAC) and Physical Layer PHY) Specifications—Amendment 4: Enhancements for Very High Throughput for Operation in Bands Below 6 GHz*, Standard IEEE Std. 802.11ac-2013, Dec. 2013.
[6] T. Murakami, M. Miyazaki, S. Ishida, and A. Fukuda, "Wireless LAN-based CSI monitoring system for object detection," *Electronics*, vol. 7, no. 11, p. 290, Nov. 2018.
[7] M. Miyazaki, S. Ishida, A. Fukuda, T. Murakami, and S. Otsuki, "Initial attempt on outdoor human detection using IEEE 802.11ac WLAN signal," in *Proc. IEEE Sensors Appl. Symp. (SAS)*, Sophia Antipolis, France, Mar. 2019, pp. 1–6.
[8] R. Takahashi, S. Ishida, A. Fukuda, T. Murakami, and S. Otsuki, "DNN-based outdoor NLOS human detection using IEEE 802.11ac WLAN signal," in *Proc. IEEE SENSORS*, Montreal, QC, Canada, Oct. 2019, pp. 1–4.
[9] T. Kanda, T. Sato, H. Awano, S. Kondo, and K. Yamamoto, "Respiratory rate estimation based on WiFi frame capture," in *Proc. IEEE 19th Annu. Consum. Commun. Netw. Conf. (CCNC)*, Jan. 2021, pp. 1–5.
[10] S. Kato, T. Fukushima, T. Murakami, H. Abeysekera, Y. Iwasaki, T. Fujihashi, T. Watanabe, and S. Saruwatari, "CSI2Image: Image reconstruction from channel state information using generative adversarial networks," *IEEE Access*, vol. 9, pp. 47154–47168, Mar. 2021.
[11] R. Kudo, K. Takahashi, T. Murakami, and T. Ogawa, "Deep learning based position estimation method using WLAN CSI feedback," *IEICE Tech. Rep.*, vol. 121, no. 173, pp. 40–45, Sep. 2021.
[12] T. Fukushima, T. Murakami, H. Abeysekera, S. Saruwatari, and T. Watanabe, "Evaluating indoor localization performance on an IEEE 802.11ac explicit-feedback-based CSI learning system," in *Proc. IEEE 89th Veh. Technol. Conf. (VTC-Spring)*, Kuala Lumpur, Malaysia, Apr. 2019, pp. 1–6.
[13] S. Kondo, S. Itahara, K. Yamashita, K. Yamamoto, Y. Koda, T. Nishio, and A. Taya, "Bi-directional beamforming feedback-based firmware-agnostic WiFi sensing: An empirical study," *IEEE Access*, vol. 10, pp. 36924–36934, Apr. 2022.
[14] M. Kotaru, K. Joshi, D. Bharadia, and S. Katti, "SpotFi: Decimeter level localization using WiFi," in *Proc. ACM Conf. Special Interest Group Data Commun.*, London, U.K., Aug. 2015, pp. 269–282.

[15] J. Xiong and K. Jamieson, "Arraytrack: A fine-grained indoor location system," in *Proc. USENIX NSDI*, Lombard, IL, USA, Apr. 2013, pp. 71–84.
[16] R. O. Schmidt, "Multiple emitter location and signal parameter estimation," *IEEE Trans. Antennas Propag.*, vol. AP-34, no. 3, pp. 276–280, Mar. 1986.
[17] H. Jiang, Z. Zhang, C.-X. Wang, J. Zhang, J. Dang, L. Wu, and H. Zhang, "A novel 3D UAV channel model for A2G communication environments using AoD and AoA estimation algorithms," *IEEE Trans. Commun.*, vol. 68, no. 11, pp. 7232–7246, Nov. 2020.
[18] L. Wan, K. Liu, Y.-C. Liang, and T. Zhu, "DOA and polarization estimation for non-circular signals in 3-D millimeter wave polarized massive MIMO systems," *IEEE Trans. Wireless Commun.*, vol. 20, no. 5, pp. 3152–3167, May 2021.
[19] Z. Tian, Z. Li, M. Zhou, Y. Jin, and Z. Wu, "PILA: Sub-meter localization using CSI from commodity Wi-Fi devices," *Sensors*, vol. 16, no. 10, p. 1664, 2016.
[20] H. F. T. Ahmed, H. Ahmad, and A. C. V., "Device free human gesture recognition using Wi-Fi CSI: A survey," *Eng. Appl. Artif. Intell.*, vol. 87, Jan. 2020, Art. no. 103281.
[21] X. Tong, H. Li, X. Tian, and X. Wang, "Triangular antenna layout facilitates deployability of CSI indoor localization systems," in *Proc. 16th Annu. IEEE Int. Conf. Sens., Commun., Netw. (SECON)*, Boston, MA, USA, Jun. 2019, pp. 1–9.
[22] X. Li, D. Zhang, Q. Lv, J. Xiong, S. Li, Y. Zhang, and H. Mei, "IndoTrack: Device-free indoor human tracking with commodity Wi-Fi," *Proc. ACM Interact., Mobile, Wearable Ubiquitous Technol.*, vol. 1, no. 3, pp. 1–22, Sep. 2017.
[23] F. Gringoli, M. Schulz, J. Link, and M. Hollick, "Free your CSI: A channel state information extraction platform for modern Wi-Fi chipsets," in *Proc. WiNTECH*, Los Cabos, Mexico, Oct. 2019, pp. 21–28.
[24] D. Halperin, W. Hu, A. Sheth, and D. Wetherall, "Tool release: Gathering 802.11n traces with channel state information," *ACM SIGCOMM Comput. Commun. Rev.*, vol. 41, no. 1, p. 53, Jan. 2011.
[25] Y. Xie, Z. Li, and M. Li, "Precise power delay profiling with commodity WiFi," in *Proc. 21st Annu. Int. Conf. Mobile Comput. Netw.*, Paris, France, Sep. 2015, pp. 53–64.
[26] A. M. Sayeed, "Deconstructing multiantenna fading channels," *IEEE Trans. Signal Process.*, vol. 50, no. 10, pp. 2563–2579, Nov. 2002.
[27] K. Miyashita, T. Nishimura, T. Ohgane, Y. Ogawa, Y. Takatori, and K. Cho, "High data-rate transmission with eigenbeam-space division multiplexing (E-SDM) in a MIMO channel," in *Proc. IEEE 56th Veh. Technol. Conf.*, Vancouver, BC, Canada, Sep. 2002, pp. 1302–1306.
[28] G. W. Stewart, "On the early history of the singular value decomposition," *SIAM Rev.*, vol. 35, no. 4, pp. 551–566, Dec. 1993.
[29] T.-J. Shan, M. Wax, and T. Kailath, "On spatial smoothing for direction-of-arrival estimation of coherent signals," *IEEE Trans. Acoust., Speech, Signal Process.*, vol. ASSP-33, no. 4, pp. 806–811, Apr. 1985.

SOHEI ITAHARA (Graduate Student Member, IEEE) received the B.E. degree in electrical and electronic engineering from Kyoto University, in 2020, where he is currently pursuing the M.I. degree with the Graduate School of Informatics.

SOTA KONDO (Graduate Student Member, IEEE) received the B.E. degree in electrical and electronic engineering from Kyoto University, in 2021, where he is currently pursuing the M.I. degree with the Graduate School of Informatics.

KOTA YAMASHITA (Student Member, IEEE) received the B.E. degree in electrical and electronic engineering from Kyoto University, in 2020, where he is currently pursuing the M.I. degree with the Graduate School of Informatics.

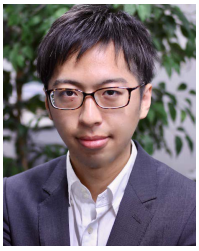

TAKAYUKI NISHIO (Senior Member, IEEE) received the B.E. degree in electrical and electronic engineering and the master's and Ph.D. degrees in informatics from Kyoto University, in 2010, 2012, and 2013, respectively. He was an Assistant Professor with the Graduate School of Informatics, Kyoto University, from 2013 to 2020. From 2016 to 2017, he was a Visiting Researcher with the Wireless Information Network Laboratory (WINLAB), Rutgers University, USA. He has been an Associate Professor with the School of Engineering, Tokyo Institute of Technology, Japan, since 2020. His current research interests include machine learning-based network control, machine learning in wireless networks, and heterogeneous resource management.

KOJI YAMAMOTO (Senior Member, IEEE) received the B.E. degree in electrical and electronic engineering and the master's and Ph.D. degrees in informatics from Kyoto University, in 2002, 2004, and 2005, respectively. From 2004 to 2005, he was a Research Fellow of the Japan Society for the Promotion of Science (JSPS). From 2008 to 2009, he was a Visiting Researcher at Wireless@KTH, Royal Institute of Technology (KTH), Sweden. Since 2005, he has been with the Graduate School of Informatics, Kyoto University, where he is currently an Associate Professor. His research interests include radio resource management, game theory, and machine learning. He is a member of the Operations Research Society of Japan. He received the PIMRC 2004 Best Student Paper Award, in 2004, and the Ericsson Young Scientist Award, in 2006. He also received the Young Researcher's Award, the Paper Award, the SUEMATSU-Yasuharu Award, the Educational Service Award from the IEICE of Japan, in 2008, 2011, 2016, and 2020, respectively, and the IEEE Kansai Section GOLD Award, in 2012. He serves as an Editor for IEEE Wireless Communications Letters, IEEE Open Journal of Vehicular Technology, Journal of Communications and Information Networks, the Symposium Co-Chair of GLOBECOM 2021, and the Vice Co-Chair of IEEE ComSoc APB CCC. He was a Tutorial Lecturer in IEEE ICC 2019.

YUSUKE KODA (Member, IEEE) received the B.E. degree in electrical and electronic engineering from Kyoto University, in 2016, and the M.E. and Ph.D. degrees in informatics from the Graduate School of Informatics, Kyoto University, in 2018 and 2021, respectively. He is currently a Postdoctoral Researcher with the Centre for Wireless Communications, University of Oulu, Finland, where he visited the Centre for Wireless Communications, in 2019, to conduct collaborative research. He received the VTS Japan Young Researcher's Encouragement Award, in 2017, and TELECOM System Technology Award, in 2020. He was a recipient of the Nokia Foundation Centennial Scholarship, in 2019.